

Biocompatible Triplex Ag@SiO₂@mTiO₂ Core–Shell Nanoparticles for Simultaneous Fluorescence-SERS Bimodal Imaging and Drug Delivery

Yunqing Wang, Lingxin Chen,* and Ping Liu^[a]

Abstract: Herein, we report the synthesis of biocompatible triplex Ag@SiO₂@mTiO₂ core–shell nanoparticles (NPs) for simultaneous fluorescence-surface-enhanced Raman scattering (F-SERS) bimodal imaging and drug delivery. Stable Raman signals were created by typical SERS tags that were composed of Ag NPs for optical enhancement, a reporter molecule of 4-mercaptopyridine (4-Mpy) for a spectroscopic signature, and a silica shell for protection. A further coating of mesoporous titania (mTiO₂) on the SERS tags offered high loading capacity for a fluorescence dye (flavin mononucleotide) and an anti-cancer drug

(doxorubicin (DOX)), thereby endowing the material with fluorescence-imaging and therapeutic functions. The as-prepared F-SERS dots exhibited strong fluorescence when excited by light at 460 nm whilst a stable, characteristic 4-Mpy SERS signal was detected when the excitation wavelength was changed to longer wavelength (632.8 nm), both in solution and after incorporation inside living cells. Their

Keywords: core–shell structures · drug delivery · fluorescence · nanoparticles · surface-enhanced Raman scattering

excellent biocompatibility was demonstrated by low cytotoxicity against MCF-7 cells, even at a high concentration of 100 μg mL⁻¹. In vitro cell cytotoxicity confirmed that DOX-loaded F-SERS dots had a comparable or even greater therapeutic effect compared with the free drug, owing to the increased cell-uptake, which was attributed to the possible endocytosis mechanism of the NPs. To the best of our knowledge, this is the first proof-of-concept investigation on a multifunctional nanomedicine that possessed a combined capacity for fast and multiplexed F-SERS labeling as well as drug-loading for cancer therapy.

Introduction

Functional nanomaterials with superior optical properties offer tremendous scope for future biomedical applications, including imaging, disease diagnosis, and drug delivery. Smart combinations of different nanostructured materials will support the development of complex nanomedical platforms, which exhibit multiple functionalities for applications that are difficult to achieve with single-component nanoparticles. Recently, extensive research has focused on multifunctional nanomedicines that are constructed from various optical nanomaterials for multimodal imaging and simultaneous diagnosis and therapy. These nanoparticles can be Au NPs,^[1] quantum dots (QDs),^[2] or Fe₃O₄ magnetic NPs^[3] that are encapsulated inside various types of polymers and inorganic shells, which endow the nanoplatform with unique optical, acoustic, and magnetic properties for clinical multi-

imaging (computed tomography, fluorescence, magnetic resonance imaging, etc.) therapeutic purposes.

Recently, the use of surface-enhanced Raman scattering (SERS) tags as nanoproboscopes for bioimaging has received increasing attention. These SERS tags are composed from metallic nanoparticles (NPs) for optical enhancement and specific organic Raman reporter molecules for producing characteristic Raman signals. SERS tags inherit the prominent advantages of ultrasensitive, quantitative, and real-time detection.^[4] Moreover, owing to the narrow SERS peaks (typically about 3 nm), they possess extraordinary multiplexing capability (they can distinguish between 10–100 targets within a single experiment) compared with classic fluorescent probes, such as QDs (3–10 targets) and organic dyes (1–3 targets);^[5] as such, these tags show great potential in multiplex biomedical analysis. Over the last decade, the application of Raman tags in cancer imaging and detection has been demonstrated at the level of various types of living cells,^[6] tissues,^[7] and living animals.^[8]

In spite of the excellent sensitivity and multiplex capability, several critical issues still need to be addressed in the SERS tag and imaging technique. One key challenge is the slow SERS imaging speed, which is a major hurdle for fast biomedical detection. To solve this problem, bifunctional fluorescence-SERS (F-SERS) dots that integrate both SERS and fluorescence moieties, together with a dual-modal imaging system, have been developed for multiple assays. In such a sensing platform, fluorescence imaging is more-intuitive

[a] Dr. Y. Wang, Prof. L. Chen, P. Liu
Key Laboratory of Coastal Zone Environmental Processes
Yantai Institute of Coastal Zone Research (YIC)
Chinese Academy of Sciences (CAS)
Shandong Provincial Key Laboratory of
Coastal Zone Environmental Processes, YICCAS
Yantai Shandong 264003
17 Chunhui Road, Yantai 264003 (P. R. China)
Fax: (+86) 535-2109130
E-mail: lxchen@yic.ac.cn

Supporting information for this article is available on the WWW under <http://dx.doi.org/10.1002/chem.201103571>.

and faster than SERS imaging; therefore, the fluorescence signal can be used as an immediate indicator of the target position, whilst the SERS signal can be subsequently used for multiplex target-discrimination and quantitation.^[9]

Another challenge facing the SERS tag is the design and application of multifunctional nanoplatforms that expand their capability from simple optical imaging to simultaneous disease diagnosis and therapy. Although recent work has reported bifunctional SERS tags that combine the molecular encoding of Raman signatures for cancer-cell detection with a remote-controlled photothermal heating ability for treatment,^[8a,10] the therapeutic effects were achieved with the aid of photothermal properties of specific noble-SERS nanosubstrates (restricted to gold nanomaterials with strong near-infrared (NIR) absorption) by using complicated external NIR laser irradiation. Thus far, there have been few attempts to design and produce a SERS-tag-based nanostructure for therapeutic drug delivery, which is more-versatile in practical applications.^[11]

Herein, we report the construction of biocompatible triplex Ag@SiO₂@mTiO₂ core-shell nanoparticles (NPs) for simultaneous fluorescence-SERS (F-SERS) bimodal imaging and drug delivery. This platform is composed of two main components: The first is a typical SERS-tag structure, which is built from a single silver NP, a 4-mercaptopyridine (4-Mpy) Raman reporter, and a thin silica layer. The second component is a mesoporous TiO₂ (mTiO₂) shell-coating on individual silica-coated SERS tags, which endows the nano-platform with the bifunctionality of fluorescent dye (flavin mononucleotide)-labeling and anti-cancer drug (doxorubicin (DOX))-loading. The as-prepared biocompatible F-SERS tags are shown to be effective vehicles for intracellular drug delivery and are easily tracked by both their strong fluorescence and SERS signals inside cells. As far as we know, this is the first reported preparation of multifunctional mesoporous-titania-coated SERS tags for both bimodal F-SERS imaging and drug delivery. By further designing multiplex barcodings with different Raman reporters and dyes, this F-SERS platform has great potential for simultaneously tracking the multiple-loaded therapeutic components by monitored distinct fluorescence and SERS signals.

Results and Discussion

Silver NPs were chosen as SERS nanosubstrates to provide strongly enhanced spectroscopic signals owing to the local optical fields present at metal surfaces (Figure 1). After the Raman reporters of 4-Mpy were added and adsorbed onto the colloidal surface, the Ag-Mpy NPs were transferred into 2-propanol to coat dense silica shells to form Ag@SiO₂ nanostructures according to the well-known Stöber method.^[12] Then, a mesoporous titania shell was deposited onto the surface of the Ag@SiO₂ NPs to form a bilayered composite nanostructure (Ag@SiO₂@mTiO₂) by the condensation of ultrasmall TiO₂ primary particles in virtue of the existence of diblock-copolymers of Lutensol ON50 (RO-(CH₂CH₂O)₅H, R < C₈H₁₇, fatty alcohol). Taking advantage of the high affinity of titania towards phosphate species, flavin mononucleotide (FMN) was incubated with Ag@SiO₂@mTiO₂ to render the SERS tags with fluorescence ability. Finally, a model anticancer drug (DOX) was loaded for therapeutic applications.

The TEM images (Figure 2 A,B) showed defined, uniform Ag@SiO₂ particles with sizes in the range 150–200 nm. The silica shell was about 60 nm in thickness. After the coating process, these core-shell tags were well-dispersed spherical nanoparticles. Figure 2C,D show TEM images of Ag@-

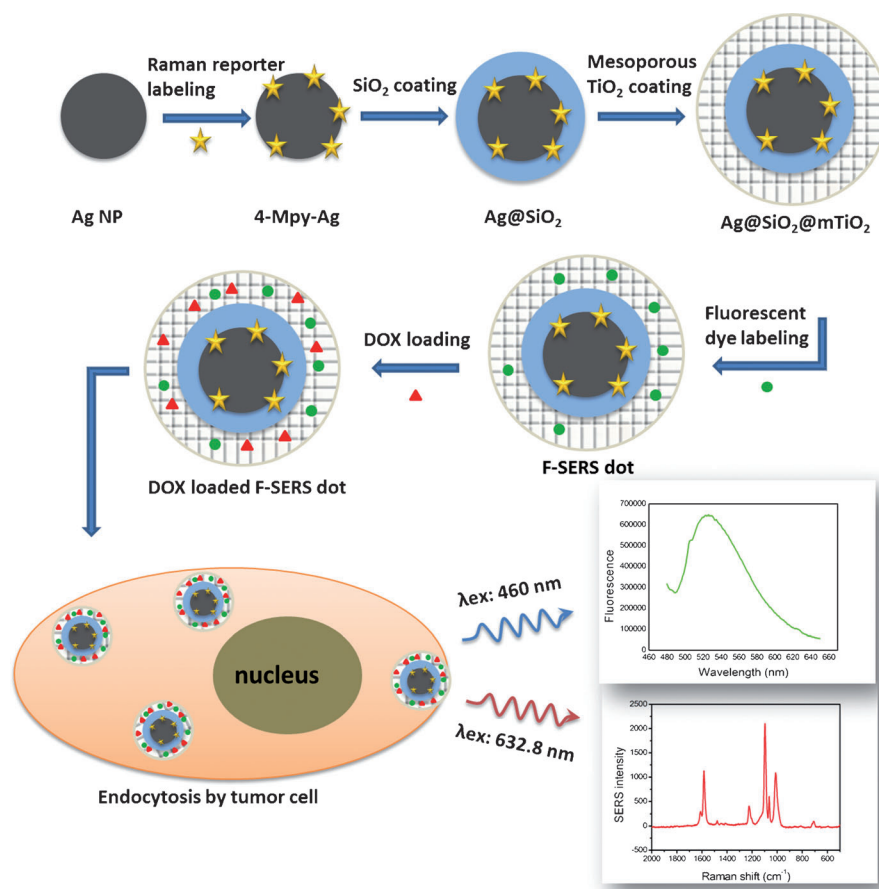


Figure 1. Preparation of DOX-loaded F-SERS dots.

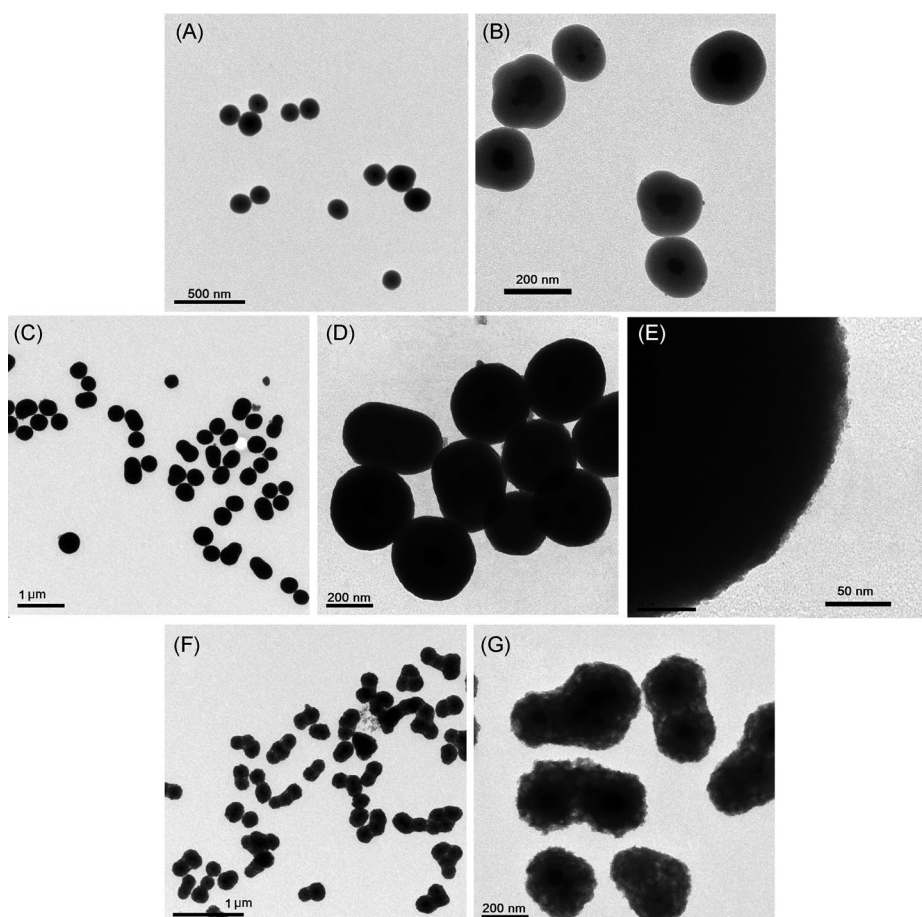


Figure 2. TEM images of sphere-shaped Ag@SiO₂ NPs (A, B) and Ag@SiO₂@mTiO₂ NPs (C, D) that were synthesized by adding Ag@SiO₂ (100 μ L) colloid into the reaction mixture (1.0 mL); large-magnification TEM images of the mesoporous TiO₂ shell (E) and Ag@SiO₂@mTiO₂ NPs (F, G) that were synthesized by adding Ag@SiO₂ colloid (200 μ L) into the reaction mixture (1.0 mL), which afforded a “peanut-shaped” morphology.

SiO₂@mTiO₂ NPs with mesoporous TiO₂ coatings. During the mTiO₂ coating process, the concentration of Ag@SiO₂ core NPs influenced the shape of the products. When the amount of Ag@SiO₂ was 100 μ L in a 1.0 mL reaction mixture, the resultant NPs were monodisperse spheres with single cores, and the particle size was in the range 300–400 nm. Furthermore, from the high-magnification TEM image (Figure 2E), disordered mesopores were distributed in the shells. When the volume of Ag@SiO₂ was increased to 200 μ L, multiple core NPs (predominantly two or three NPs) were encapsulated in the mTiO₂ shell, thus forming an interesting “peanut-shaped” morphology. Moreover, the mTiO₂ shell was much thicker (almost 30 nm), with an apparent mesoporous structure (Figure 2F, G).

Although the mechanism for the formation of mesoporous titania shells is still not completely understood, it is commonly regarded that the diblock-copolymer of Lutensol ON50 is essential for acquiring the porous structure. Upon hydrolysis of tetrabutyl titanate (TBT) in trace amounts of water, the hydrophilic part of Lutensol ON50 interacts with the surface of the small primary TiO₂ NPs whilst the hydrophobic part extends into the medium, and steric stabilization

prevents the formation of larger particles.^[13] The stabilized primary particles continue to aggregate on the Ag@SiO₂ surface with polymer building in. Therefore, at the end of the reaction, the resultant TiO₂ shells are porous and the porosity is determined by the polymer type and length. It has been reported that a mTiO₂ structure that was synthesized with Lutensol ON50 has a N₂ Brunauer–Emmett–Teller (BET) surface area of 273 m²g⁻¹ and a Barret–Joyner–Halenda (BJH) adsorption average pore diameter of 1.68 nm,^[14] which would be suitable for subsequent fluorescent-dye- and drug loading.

Figure 3A shows the plasmon peak of Ag-Mpy NPs in water (centered at 424 nm), which shifted upon encapsulation in SiO₂ (471 nm), owing to the change in the dielectric environment. Further surface coating with a mTiO₂ shell induced strong end-absorption at 325 nm, and the Ag@SiO₂ cores only exhibited a shoulder in the range 400–650 nm. In Figure 3B, line a shows the SERS spectra of Ag@SiO₂ NPs recorded in ethanol. The Raman band at 1006 cm⁻¹ was assigned to the ring-breathing vibration of Raman-reporter 4-Mpy, whilst the band at 1097 cm⁻¹ was assigned to the C–S stretching mode. The peaks at 1220 and 1583 cm⁻¹ were attributed to the C–H in-plane-bending stretch and the ring-stretch mode, respectively.^[15] SERS spectra of Ag@SiO₂@mTiO₂ (lines (b) and (c)) showed that the TiO₂ coating did not affect the SERS signature of the Raman reporter.

In this nanoplatform, SiO₂ and mTiO₂ shells were both essential to achieve the desired multiple functions. SiO₂ coating played four roles: 1) It provided good dispersity of the NPs in organic solvent, which was important for the formation of a uniform structure in the subsequent TiO₂-coating process in ethanol. Unprotected Ag-MPy NPs tended to show uncontrolled aggregation, which led to a lack of synthetic reproducibility. 2) It effectively reduced the potential cytotoxicity of Ag NPs owing to the oxidative effect in living cells.^[16] 3) Metal NPs quenched the fluorescence of fluorophores in close proximity to themselves. Herein, the Ag NPs and adsorbed FMN dye molecules in mesoporous TiO₂ were sandwiched by the 60 nm-thick SiO₂ coating,

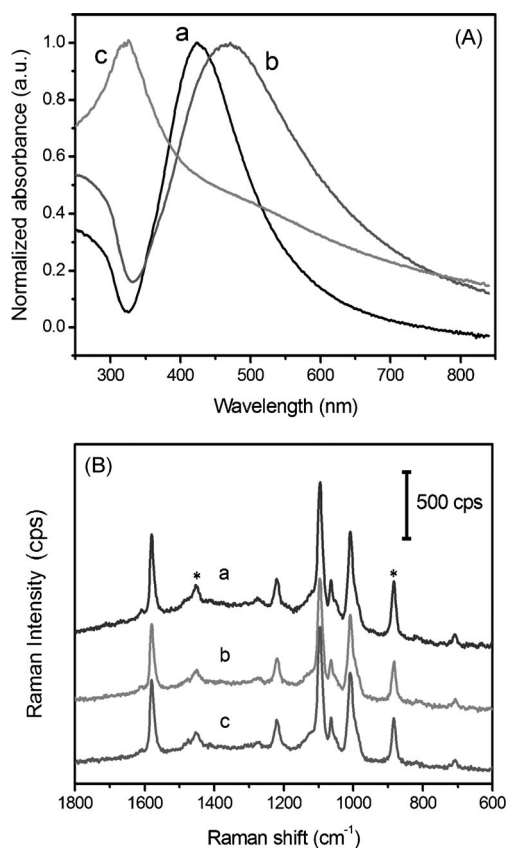


Figure 3. A) Normalized UV/Vis absorption spectra of Ag-Mpy (a), Ag@SiO₂ (b), and Ag@SiO₂@mTiO₂ NPs (c) in water; B) SERS spectra of Ag@SiO₂ (a) and Ag@SiO₂@mTiO₂ NPs (b), which were synthesized by adding 100 μ L Ag@SiO₂ colloid into the reaction mixture (1.0 mL), and Ag@SiO₂@mTiO₂ NPs (c), which were synthesized by adding 200 μ L Ag@SiO₂ colloid into the reaction mixture (1.0 mL). The asterisks indicate the characteristic Raman peak (1455 and 885 cm⁻¹) of EtOH.

which efficiently prevented this quenching effect and preserved the fluorescence signal of the tags.^[9b] 4) Most importantly, silica-encapsulation greatly enhanced the stability of the SERS signal of the tags. When unprotected SERS tags were used in bioimaging, they were heavily influenced by their surroundings: not only the replacement of the Raman reporters by endogenous small thio-molecules, but also by the unwanted signal from the cell components. A condensed silica shell prevented their impermeability to attach onto the surface of the metal cores.^[12,17]

To test the stability of the SERS signal of the particles, an interference experiment was performed by using Ag@-SiO₂@mTiO₂ and Ag@mTiO₂ NPs, which did not contain the middle SiO₂ layer (the TiO₂ shells were coated by using a similar procedure but with Ag-Mpy NPs instead of Ag@SiO₂; see the Supporting Information, Figure S1). Although the SERS intensity of Ag@mTiO₂ NPs was stronger because of the aggregation of Ag NPs—that is, more “hot-spots” in ethanol—after adding four different small thio-molecules, the signals decreased dramatically over a short space of time owing to their penetration into the porous shell and the displacement of 4-Mpy Raman reporters (Fig-

ure 4A). Interestingly, the addition of thio-BSA (which can cause a decrease in the SERS peak of uncoated Ag-Mpy; data not shown) did not affect the SERS signal, presumably because the size of BSA (hydrodynamic diameter = 7.0 nm^[18]) was larger than that of the mesopores (about 2 nm) and was therefore blocked by the mTiO₂ shell. Comparatively, all of the thio-molecules caused no apparent change in the Mpy spectrum of Ag@SiO₂@mTiO₂ NPs (Figure 4B). This result conclusively showed that the Raman reporters were “locked in”, whilst external molecules were “locked out” by the silica shell.

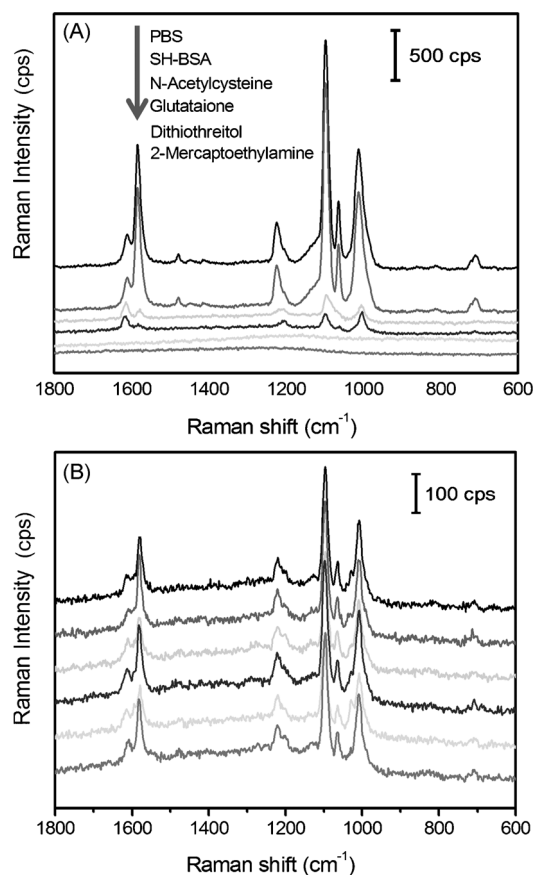


Figure 4. Comparison of the stabilities of the SERS signals of Ag@mTiO₂ (A) and Ag@SiO₂@mTiO₂ NPs (B) upon the interference of thio-molecules. The concentrations of *N*-acetylcysteine, glutathione, dithiothreitol, and 2-mercaptoethylamine was 2.5 mM, and the concentration of denatured bovine serum albumin (thio-BSA) was 0.5 mg mL⁻¹.

Mesoporous TiO₂ as the second shell in this nanoplatfrom made this system particularly suitable as fluorescent dyes and drug carriers. Inorganic mesoporous materials, such as mesoporous silica,^[19] mesoporous carbon,^[20] and CaCO₃^[21] have exhibited various advantages compared to organic materials, such as high chemical/thermal stability, high drug-loading capability, and rich surface-chemical functionalities for possible molecular recognition and targeted delivery. More recently, TiO₂ nanomaterials, including as TiO₂ NPs,^[22] whiskers,^[23] and shells^[24] have received much attention in

clinical applications, and mesoporous TiO₂ particles have also been found to be biocompatible loading vehicles for intracellular drug delivery.^[25] In addition, compared with other inorganic materials, TiO₂ NPs have a unique property: high affinity toward phosphate species through Ti–O–P and P=O bonds.^[25,26] To take advantage of this property in bioimaging, herein, we used flavin mononucleotide (FMN or Riboflavin 5P', a derivative of Riboflavin) for the fluorescent labeling of SERS tags, which could strongly attach onto the mesoporous TiO₂ shell through simple mixing.

As shown in Figure 5, lines a and b represent the UV/Vis absorption of solutions of FMN before and after incubation with Ag@SiO₂@mTiO₂ NPs. The decrease in absorbance at

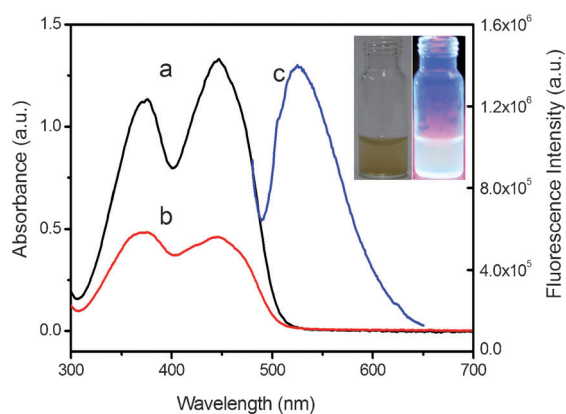


Figure 5. UV/Vis absorption of a solution of FMN (2.5×10^{-4} M) a) before and b) after incubation with Ag@SiO₂@mTiO₂ NPs; c) fluorescence spectrum of a solution of F-SERS tags ($100 \mu\text{g mL}^{-1}$). Inset: solution of F-SERS tags under sunlight and 365 nm UV-light excitation.

447 nm in the supernatant confirmed the adsorption of FMN onto mTiO₂ shells, and the maximum amount of FMN per gram of NPs was determined to be 0.19 mmol. The FMN-labeled NPs displayed the typical emission of FMN at 530 nm (Figure 5, line c). Under UV-light excitation, the colloid exhibited a bright-green color (Figure 5, inset). The F-SERS dots were checked to ensure that there was no apparent desorption of FMN from the mTiO₂ shells, even after 7 days. Such a simple mixing process has an advantage over the previously used processes (covalent dye-conjugated silane chemistry^[27,9a] or dye-conjugated polyelectrolyte adsorption^[28]) that were complicated and time-consuming. As expected, fluorescence from FMN was obtained without a detectable SERS signal when the probe was excited by light at 460 nm, whilst strong SERS signals from 4-Mpy were detected without fluorescence when the tag was excited by light at 632.8 nm.

To evaluate the drug-loading capacity of as-prepared F-SERS dots, anticancer drug DOX was chosen as a model drug, and UV/Vis absorption spectroscopy was used to determine the effective DOX-storage capacity of the NPs. Figure 6A shows the UV/Vis absorption spectra of an aqueous solution of DOX before and after the interaction with F-SERS dots. The absorption intensity of DOX decreased

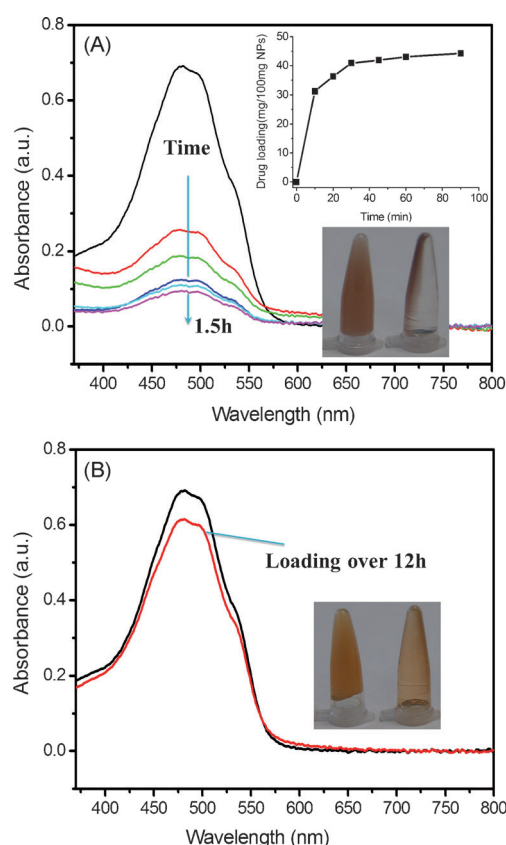


Figure 6. Normalized UV/Vis absorption spectra of DOX molecules for separated supernatant solutions after various loading times for A) Ag@SiO₂@mTiO₂ NPs and B) Ag@SiO₂ NPs. Inset in (A): Loading profile of DOX molecules with time. Photographs in (A) and (B) show DOX-loaded NPs before (left) and after (right) centrifugation.

after the interaction with NPs, thereby indicating a significant decrease in its concentration in solution; namely, DOX had been stored in NPs with a high efficiency. The mass of the DOX molecules that was loaded into F-SERS dots was estimated to be 44.2 mg/100 mg. For comparison, we also measured the coupling capacity of DOX molecules in the Ag@SiO₂ NPs without mTiO₂ coatings (Figure 6B). The results showed that the maximum payload after 12 h was only 4.9 mg per 100 mg of NPs, which was far less than that of Ag@SiO₂@mTiO₂ NPs. This distinction was also observed by the color change of the precipitate from yellow (Ag@SiO₂, the supernatant was the orange color of DOX) to brown (Ag@SiO₂@mTiO₂, the supernatant was nearly colorless) after absorbing DOX (Figure 6, picture insets). Therefore, the high drug-loading capacity and efficiency of F-SERS dots was attributed to the enhanced surface area and to the formation of cavities in the mTiO₂ shell, which left more room for drug-molecule storage through electrostatic interactions between positively charged DOX molecules and negatively charged mTiO₂ surfaces. The DOX-loaded F-SERS tags also exhibited the fluorescence of DOX molecules when excited at 479 nm (see the Supporting Information, Figure S2). However, there was a significant quenching compared with the strong emission of free DOX

in solution, which was because DOX was concentrated in the mTiO₂ shells, thereby leading to radiationless energy-transfer between DOX molecules.^[19d] Moreover, the loading of DOX did not induce any variation in the 4-MPy SERS spectrum of the tags.

To verify the intracellular delivery of DOX, confocal laser scanning microscopy (CLSM) images were taken of MCF-7 cells after treatment with DOX-loaded F-SERS dots for 24 h (Figure 7). When the excitation was set at 488 nm, the

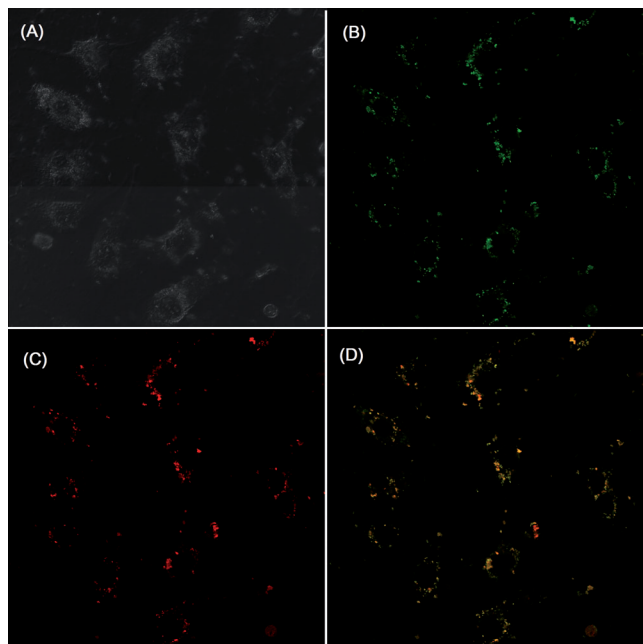


Figure 7. Confocal images of MCF-7 cells that were treated with DOX-loaded F-SERS dots (20 μg mL⁻¹) for 24 h: A) bright-field image; B) green fluorescence of FMN in F-SERS dots; C) red fluorescence of DOX-loaded molecules; and D) a composite image. The overlapping of green and red is shown in yellow.

green fluorescence that resulted from FMN-labeled NPs was visualized in the cytoplasm. The discrete green dots indicated that the FMN molecules remained inside the titania shells without much leaching. When the excitation was set at 543 nm, the red fluorescence of DOX in MCF-7 cells was observed. A composite image confirmed that the anticancer drug was indeed delivered by the F-SERS tags. After NP treatment, the cell membranes had shrunk and the morphology of the cells became round in shape, thus indicating a DOX-induced cell apoptosis.

Furthermore, we investigated the intracellular SERS performance of the drug-loaded dual-mode image probe by Raman microscopy by changing the excitation wavelength to 632.8 nm. Figure 8 shows a dark-field image of the living MCF-7 cells after incubation with drug-loaded F-SERS dots for 24 h, and SERS spectra at five different laser spots across one cell. Obviously, strong SERS signals were recorded from NPs clusters that had accumulated in cytoplasm, whilst the signals at the nucleus and the culture medium

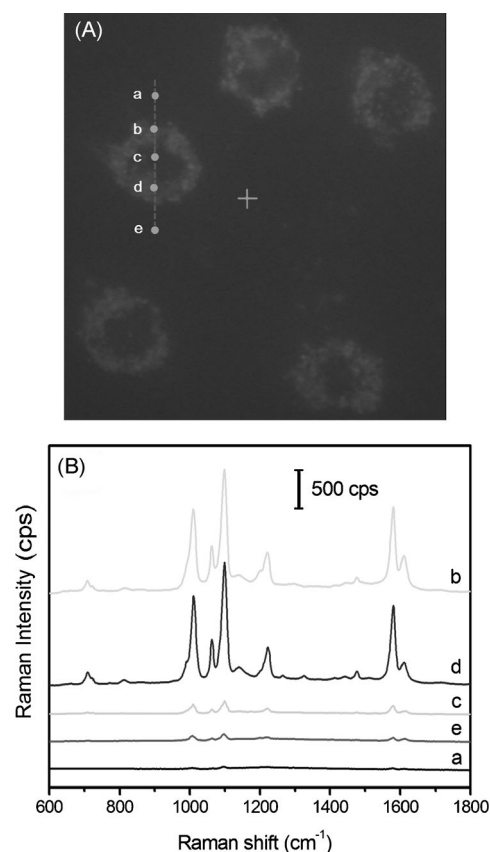


Figure 8. A) Dark-field images of MCF-7 cells after incubating DOX-loaded F-SERS dots for 24 h; B) corresponding Raman spectra at five different laser spots across one F-SERS-dot-labeled MCF-7 cell.

were much weaker. Besides, the characteristic Raman signal of 4-Mpy from the F-SERS tags remained robust and no obvious interference Raman peaks or fluorescence background were obtained.

Finally, we investigated the biocompatibility of F-SERS dots as bimodal cell-imaging probes and drug-delivery vehicles, as well as the therapeutic effects after DOX loading. Figure 9A shows that the MCF-7 cells that were grown in the presence of the F-SERS dot solutions retained high cell-viability in MTT assays. The cell-viabilities of the nanoparticles that were cultured in the tumor cells were above 80%, which demonstrated that the drug carriers had little cytotoxicity, even at high concentrations (100 μg mL⁻¹) and may be safe for in vitro and in vivo experiments. The low toxicological effects may be ascribed to the biocompatible and non-toxic nature of the SiO₂ bilayer and the mesoporous TiO₂ shells. To verify whether the released DOX was pharmacologically active, the cytotoxic effect of the DOX-loaded F-SERS dots was tested against MCF-7 cells. As shown in Figure 9B, DOX-loaded F-SERS dots exhibited comparative or even higher cytotoxicity (at high concentrations of 2.0 and 4.0 × 10⁻⁶ M) than free DOX towards MCF-7 cells, which indicated that the loaded drug retained its pharmaceutical activity.

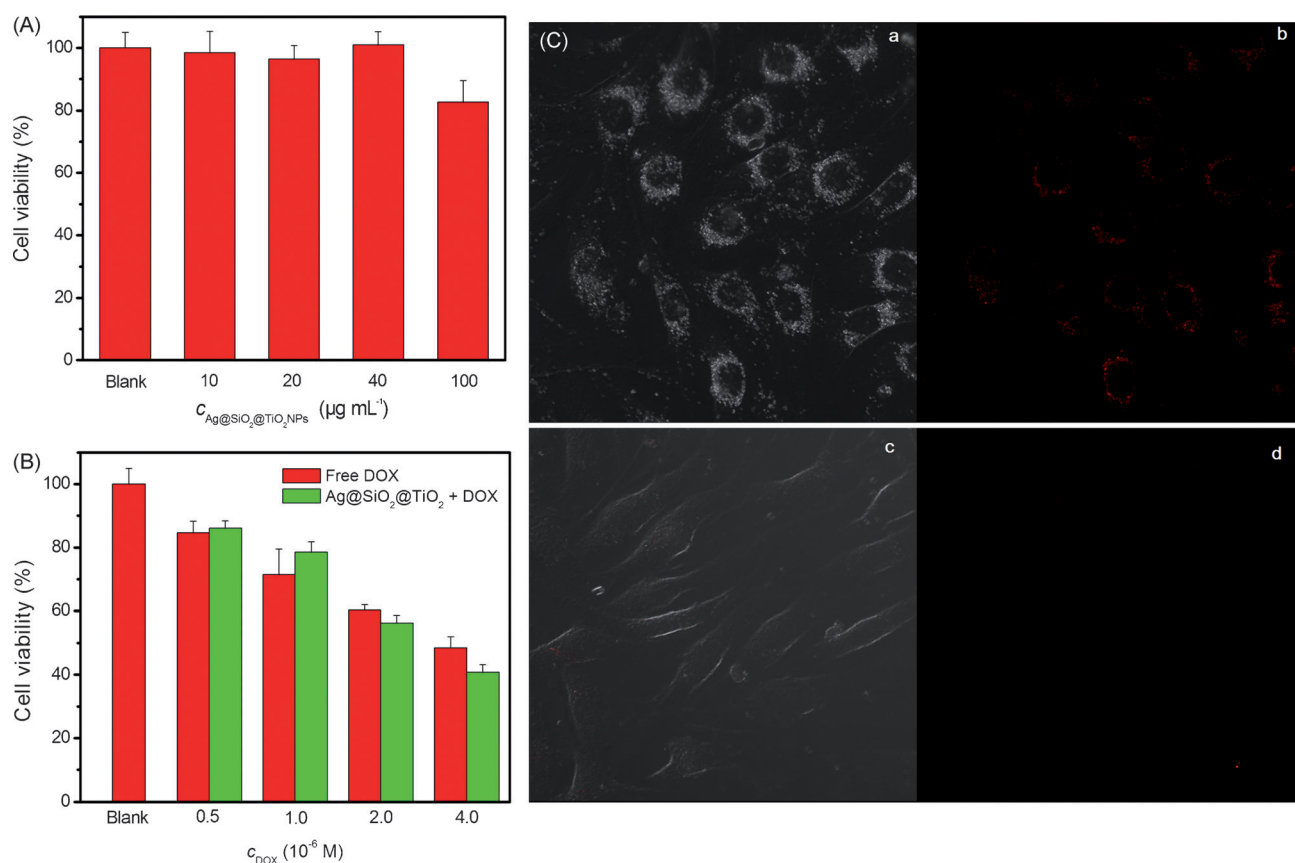


Figure 9. Cell viabilities of A) F-SERS dots and B) free DOX and DOX-loaded F-SERS dots against MCF-7 cells at different concentrations for 48 h; C) bright-field images and CLSM images of DOX-loaded F-SERS dots (a, b) and free DOX-treated cells (c, d) for 4 h.

The higher cellular accumulation of DOX from F-SERS tags might be partly attributed to the different cell-uptake mechanisms between free DOX and DOX-loaded nanocarriers.^[19a] For free DOX, the cell-uptake mechanism was a passive-diffusion process, whilst for DOX-loaded carriers, a possible endocytosis mechanism was involved, which was more-effective than the passive diffusion process. CLSM images of the treated cells after 4 h (Figure 9C) revealed that an abundance of DOX (bright red fluorescence) had been rapidly delivered into the cells by the NPs, which sustainably released it and then migrated into the nucleus. By contrast, very limited amounts of free DOX diffused into the cells and the fluorescence was hardly detectable. Thus, the higher uptake of DOX-containing nanocarriers by the MCF-7 cells should be responsible for the enhanced DOX cytotoxicity and cell-death. On the other hand, when the cancer cells were treated with free DOX, the development of multidrug resistance of cancer cells, which resulted from the expression of *p*-glycoprotein pump in the cell membrane, hampered the drug action by pumping out drug molecules from the cytosol to the extracellular area.^[3b] However, the uptake of the drug-loaded nanocarriers within the cancer cells might, to some extent, circumvent the MRD effect.^[3b, 19b, 29]

Conclusion

We have developed biocompatible triplex Ag@SiO₂@mTiO₂ core–shell NPs for simultaneous F-SERS bimodal imaging and drug delivery. In this nanoplatform, strong fluorescence was observed when excited by light at 460 nm, whilst a stable, characteristic SERS signal was detected when the excitation wavelength changed to 632.8 nm, both in solution and after being incorporated inside living cells. Moreover, F-SERS dots exhibited high drug-storage capacity and biocompatibility. In vitro cell-cytotoxicity tests on cancer cells showed that drug-loaded tags exhibited comparable or even-better therapeutic effects compared with the free drug, owing to the increased cell-uptake of the anticancer drug, which was attributed to the possible endocytosis mechanism of NPs. Overall, the designed nanoplatform is an ideal candidate for simultaneous bimodal imaging and drug delivery for cancer therapy.

Although this report describes a proof-of-concept study of multiplex F-SERS dots with combined therapeutic function, we believe that this F-SERS platform has broad applications as a drug-delivery system. First, by judicious surface modification with tumor-targeting molecules, the therapeutic selectivity of the nanomedicine would be greatly improved, thereby reducing the side-effects of chemotherapeutic drugs to normal cells and tissues. Second, after designing multiplex

barcodings with different Raman reporters and dyes, these systems could simultaneously track the multiple components by monitored distinct fluorescence and SERS signals. Moreover, by expanding the fluorescence and SERS signals to the near-infrared region, this nanoplatform also has great potential for the study of transport- and distribution behavior of multiple drugs for tumor diagnosis and therapy in living animals, which may be helpful for the high-throughput screening of drugs and nanoparticle formulations.

Experimental Section

Materials: Silver nitrate, hydroxylamine hydrochloride, tetraethoxyorthosilicate (TEOS), tetrabutyl titanate (TBT), and 2-propanol were purchased from Sinopharm Chemical Reagent Co., Ltd. Nonionic surfactant Lutensol ON50 was obtained from BASF. 4-mercaptopyridine (4-Mpy), flavin mononucleotide (FMN), doxorubicin hydrochloride (DOX), *N*-acetylcysteine, glutathione, dithiothreitol, and 2-mercaptoethylamine were obtained from Sigma–Aldrich. Denatured bovine serum albumin (thio-BSA) was prepared by treating BSA with NaBH_4 accordingly to a literature procedure.^[30] Deionized water ($18.0 \text{ M}\Omega \text{ cm}^{-1}$) was used in all of the experiments.

Characterization: The TEM images were acquired on a JEM-1400 transmission electron microscope (JEOL, Japan). UV/Vis absorption spectra were recorded on a Thermo Scientific NanoDrop 2000/2000C spectrophotometer. SERS spectra were recorded by using a DXR Raman Microscope (Thermo Fisher, USA). A 632.8 nm diode pumped He:Ne laser was focused by a $\times 50$ microscope objective with a power of 5 mW. The exposure time was 4 s and each of the signals were collected twice. Fluorescence measurements were carried out on a FluoroMax-4 spectrofluorometer (HORIBA, France). Confocal laser scanning microscopy (CLSM) was operated on an Olympus Fluoview FV1000 (Japan).

Preparation of Ag colloids: Silver NPs were prepared by the reduction of silver nitrate with hydroxylamine hydrochloride at RT, according to the method described previously by Lendl and Leopold.^[31] Briefly, 11.6 mg of $\text{NH}_2\text{OH}\cdot\text{HCl}$ was dissolved in H_2O (100 mL) and was mixed with 0.1 M NaOH (3.3 mL). Then, to 9 mL of the above solution, was added 10 mM AgNO_3 (1 mL) under gentle stirring at RT. A rapid color change was observed, and finally a clear brownish-yellow Ag colloid was obtained.

Preparation of SERS tags (Ag@SiO₂ NP): Silica-coated SERS tags were prepared according to the method reported by Liu et al.^[12] In a typical procedure, a solution of Raman-reporter molecule 4-Mpy (10^{-5} M) was gently mixed with silver colloids (10 mL) and allowed to stand for 30 min. Then, the mixture was slowly added to 2-propanol ($\text{H}_2\text{O}/2\text{-propanol}$, ratio maintained at 1:5). Under gentle stirring, ammonia (1.5 mL, 25 wt %) and TEOS (20 μL) were added consecutively. The reaction was stirred overnight at RT. The tags were separated from the reaction mixture by centrifugation for 10 min at 7000 rpm, washed twice with EtOH, and then redispersed in EtOH (1 mL).

Preparation of Ag@SiO₂@mTiO₂ NPs: A typical procedure for coating Ag@SiO₂ particles with mTiO₂ is as follows.^[32] Firstly, a 0.1 M aqueous solution of Lutensol ON50 (4 μL) was dissolved in a pre-mixed dispersion of Ag@SiO₂ core particles (100 or 200 μL) in EtOH (500 μL). Then, a further 500 μL of EtOH was mixed with TBT (10 μL). This diluted titania precursor solution was then added to the dispersion of core particles, followed by vigorous shaking. The mixture was sonicated for at least 20 min in an ultrasound bath before being left overnight to allow the reaction to go to completion. The mesoporous-titania-coated particles (Ag@SiO₂@mTiO₂ NPs) were washed twice with EtOH and water.

Preparation of F-SERS dots: The Ag@SiO₂@mTiO₂ NPs (1 mL) were centrifuged and redispersed into a solution of flavin mononucleotide in water (FMN; $2.5 \times 10^{-4} \text{ M}$, 1 mL). After stirring for 12 h, the product was collected by centrifugation, and the supernatant was then removed for UV/Vis measurements. A stock solution of FMN ($2.5 \times 10^{-4} \text{ M}$) was used

as a standard and was serially diluted to concentrations of $1.56\text{--}12.5 \times 10^{-5} \text{ M}$ in deionized water. The decrease in the absorbance in the supernatant at 447 nm represented the adsorption of FMN onto Ag@SiO₂@TiO₂ NPs.

Anti-cancer-drug (doxorubicin) loading: FMN-labeled Ag@SiO₂@mTiO₂ NPs (F-SERS dots, 200 μL) was centrifuged and redispersed into a solution of DOX in water (10^{-4} M , 1 mL). After different incubation times, the NPs were centrifuged and the supernatant was subjected to UV/Vis analysis to determine the amount of loaded DOX. A stock solution of DOX (10^{-4} M) was used as a standard and was serially diluted to concentrations of $5.0\text{--}100 \times 10^{-6} \text{ M}$ in deionized water. DOX solutions of different concentration were measured at 480 nm and a linear fit of the data was created and used as standard curve for the absorption against DOX concentration.

Cell culture: A breast-cancer-cell line (MCF-7) was grown as a monolayer in a humidified incubator at 37°C in air/CO₂ (95:5) in an RPMI-1640 medium that was supplemented with 10% fetal bovine serum. For all experiments, the cells were harvested by using trypsin and were resuspended in fresh medium before plating.

Cell uptake: MCF-7 cells ($1.0 \times 10^5 \text{ mL}^{-1}$) were seeded onto glass coverslips in a 24-well plate in RPMI-1640 medium that contained 10% fetal bovine serum for 24 h at 37°C in a humidified atmosphere with 5% CO₂ to allow the cells to attach. The medium was then replaced with a culture-serum-free medium (1 mL) that contained DOX-loaded F-SERS dots (50 $\mu\text{g mL}^{-1}$ with 10^{-5} M DOX). After incubation for 24 h, the cell monolayer on the cover-slip was repeatedly washed with PBS to remove the remaining particles and dead cells and then sealed with a glass microscope slide. Observations were performed by confocal laser scanning microscopy (CLSM) or by Raman microscopy.

Cytotoxicity of DOX-loaded F-SERS dots: 8×10^3 MCF-7 cells were plated in 96-well plates and incubated for 24 h to allow the cells to attach. Free DOX, and DOX-loaded F-SERS dots (the concentration of NP carriers was set at 20 $\mu\text{g mL}^{-1}$) with various DOX concentrations. Then, the cells were incubated at 37°C for a further 48 h. Cell-survival efficiency was measured by using an MTT assay, according to the manufacturer's suggested procedures. The data were the mean values of five measurements. In a separate experiment, the cells were exposed to F-SERS dots without DOX-loading in the concentration range 10–100 $\mu\text{g mL}^{-1}$. The cell-survival efficiency was measured after the incubation at 37°C for 48 h.

Acknowledgements

We acknowledge financial support from the National Natural Science Foundation of China (20975089, 81102415), the Natural Science Foundation of Shandong Province of China (ZR2010BQ012), the Science and Technology Development Plan of Yantai (2011071), and the One Hundred Person Project of the Chinese Academy of Sciences.

- [1] a) R. Guo, L. Zhang, H. Qian, R. Li, X. Jiang, B. Liu, *Langmuir* **2010**, *26*, 5428–5434; b) X. Li, J. Guo, J. Asong, M. A. Wolfert, G. J. Boons, *J. Am. Chem. Soc.* **2011**, *133*, 11147–11153; c) P. F. Jiao, H. Y. Zhou, L. X. Chen, B. Yan, *Curr. Med. Chem.* **2011**, *18*, 2086–2102.
- [2] a) Y. Guo, D. L. Shi, H. S. Cho, Z. Y. Dong, A. Kulkarni, G. M. Pauletto, W. Wang, J. Lian, W. Liu, L. Ren, Q. Q. Zhang, G. K. Liu, C. Huth, L. M. Wang, R. C. Ewing, *Adv. Funct. Mater.* **2008**, *18*, 2489–2497; b) S. H. Hu, K. T. Kuo, W. L. Tung, D. M. Liu, S. Y. Chen, *Adv. Funct. Mater.* **2009**, *19*, 3396–3403.
- [3] a) J. Kim, H. S. Kim, N. Lee, T. Kim, H. Kim, T. Yu, I. C. Song, W. K. Moon, T. Hyeon, *Angew. Chem.* **2008**, *120*, 8566–8569; *Angew. Chem. Int. Ed.* **2008**, *47*, 8438–8441; b) J. Kim, J. E. Lee, S. H. Lee, J. H. Yu, J. H. Lee, T. G. Park, T. Hyeon, *Adv. Mater.* **2008**, *20*, 478–483.

- [4] a) T. Lou, Y. Wang, J. Li, H. Peng, H. Xiong, L. Chen, *Anal. Bioanal. Chem.* **2011**, *401*, 333–338; b) J. Li, L. Chen, T. Lou, Y. Wang, *ACS Appl. Mater. Interfaces* **2011**, *3*, 3936–3941.
- [5] S. Schlücker, *ChemPhysChem* **2009**, *10*, 1344–1354.
- [6] a) H. Park, S. Lee, L. Chen, E. K. Lee, S. Y. Shin, Y. H. Lee, S. W. Son, C. H. Oh, J. M. Song, S. H. Kang, J. Choo, *Phys. Chem. Chem. Phys.* **2009**, *11*, 7444–7449; b) H. Chon, S. Lee, S. W. Son, C. H. Oh, J. Choo, *Anal. Chem.* **2009**, *81*, 3029–3034; c) S. Lee, S. Kim, J. Choo, S. Y. Shin, Y. H. Lee, H. Y. Choi, S. Ha, K. Kang, C. H. Oh, *Anal. Chem.* **2007**, *79*, 916–922; d) M. Y. Sha, H. Xu, M. J. Natan, R. Cromer, *J. Am. Chem. Soc.* **2008**, *130*, 17214; e) L. Y. Wu, B. M. Ross, S. Hong, L. P. Lee, *Small* **2010**, *6*, 503–507; f) D. C. Kennedy, K. A. Hoop, L. L. Tay, J. P. Pezacki, *Nanoscale* **2010**, *2*, 1413–1416.
- [7] a) S. Schlücker, B. Küstner, A. Punge, R. Bonfig, A. Marx, P. Ströbel, *J. Raman Spectrosc.* **2006**, *37*, 719–721; b) B. Lutz, C. Dentinger, L. Sun, L. Nguyen, J. Zhang, A. Chmura, A. Allen, S. Chan, B. Knudsen, *J. Histochem. Cytochem.* **2007**, *56*, 371–379; c) B. Küstner, M. Gellner, M. Schütz, F. Schöppler, A. Marx, P. Ströbel, P. Adam, C. Schmuck, S. Schlücker, *Angew. Chem.* **2009**, *121*, 1984–1987; *Angew. Chem. Int. Ed.* **2009**, *48*, 1950–1953.
- [8] a) G. von Maltzahn, A. Centrone, J. H. Park, R. Ramanathan, M. J. Sailor, T. A. Hatton, S. N. Bhatia, *Adv. Mater.* **2009**, *21*, 3175–3180; b) X. Qian, X. H. Peng, D. O. Ansari, Q. Yin-Goen, G. Z. Chen, D. M. Shin, L. Yang, A. N. Young, M. D. Wang, S. Nie, *Nat. Biotechnol.* **2008**, *26*, 83–90.
- [9] a) M. A. Woo, S. M. Lee, G. Kim, J. Baek, M. S. Noh, J. E. Kim, S. J. Park, A. Minai-Tehrani, S. C. Park, Y. T. Seo, Y. K. Kim, Y. S. Lee, D. H. Jeong, M. H. Cho, *Anal. Chem.* **2009**, *81*, 1008–1015; b) Z. Y. Wang, H. Wu, C. L. Wang, S. H. Xu, Y. P. Cui, *J. Mater. Chem.* **2011**, *21*, 4307–4313.
- [10] a) W. Lu, A. K. Singh, S. A. Khan, D. Senapati, H. Yu, P. C. Ray, *J. Am. Chem. Soc.* **2010**, *132*, 18103–18114; b) L. Beqa, Z. Fan, A. K. Singh, D. Senapati, P. C. Ray, *ACS Appl. Mater. Interfaces* **2011**, *3*, 3316–3324.
- [11] A. M. Fales, H. Yuan, T. Vo-Dinh, *Langmuir* **2011**, *27*, 12186–12190.
- [12] X. Liu, M. Knauer, N. P. Ivleva, R. Niessner, C. Haisch, *Anal. Chem.* **2010**, *82*, 441–446.
- [13] S. Eiden-Assmann, J. Widoniak, G. Maret, *Chem. Mater.* **2004**, *16*, 6–11.
- [14] A. F. Demirörs, A. van Blaaderen, A. Imhof, *Chem. Mater.* **2009**, *21*, 979–984.
- [15] a) H. Z. Yu, N. Xia, Z. F. Liu, *Anal. Chem.* **1999**, *71*, 1354–1358; b) X. Q. Fu, F. L. Bei, X. Wang, X. J. Yang, L. D. Lu, *J. Raman Spectrosc.* **2009**, *40*, 1290–1295.
- [16] a) P. V. AshaRani, G. Low Kah Mun, M. P. Hande, S. Valiyaveetil, *ACS Nano* **2009**, *3*, 279–290; b) S. T. Selvan, T. T. Tan, J. Y. Ying, *Adv. Mater.* **2005**, *17*, 1620–1630; c) A. Guerrero-Martínez, J. Pérez-Juste, L. M. Liz-Marzán, *Adv. Mater.* **2010**, *22*, 1182–1195.
- [17] W. E. Doering, S. M. Nie, *Anal. Chem.* **2003**, *75*, 6171–6176.
- [18] A. D. Chen, D. H. Wu, C. S. Johnson, *J. Phys. Chem.* **1995**, *99*, 828–834.
- [19] a) Y. Chen, H. Chen, D. Zeng, Y. Tian, F. Chen, J. Feng, J. Shi, *ACS Nano* **2010**, *4*, 6001–6013; b) H. Meng, M. Liang, T. Xia, Z. Li, Z. Ji, J. I. Zink, A. E. Nel, *ACS Nano* **2010**, *4*, 4539–4550; c) F. H. Chen, L. M. Zhang, Q. T. Chen, Y. Zhang, Z. J. Zhang, *Chem. Commun.* **2010**, *46*, 8633–8635; d) T. Wang, F. Chai, Q. Fu, L. Zhang, H. Liu, L. Li, Y. Liao, Z. Su, C. Wang, B. Duan, D. Ren, *J. Mater. Chem.* **2011**, *21*, 5299–5306.
- [20] T. W. Kim, P. W. Chung, S. Y. Slowing, M. Tsunoda, E. S. Yeung, V. S. Lin, *Nano Lett.* **2008**, *8*, 3724–3727.
- [21] W. Wei, G. H. Ma, G. Hu, D. Yu, T. McLeish, Z. G. Su, Z. Y. Shen, *J. Am. Chem. Soc.* **2008**, *130*, 15808–15810.
- [22] T. Paunesku, S. Vogt, B. Lai, J. Maser, N. Stojicevic, K. T. Thurn, C. Osipo, H. Liu, D. Legnini, Z. Wang, C. Lee, G. E. Woloschak, *Nano Lett.* **2007**, *7*, 596–601.
- [23] Q. Li, X. Wang, X. Lu, H. Tian, H. Jiang, G. Lv, D. Guo, C. Wu, B. Chen, *Biomaterials* **2009**, *30*, 4708–4715.
- [24] I. L. Hsiao, Y. J. Huang, *Chem. Res. Toxicol.* **2011**, *24*, 303–313.
- [25] K. C. Wu, Y. Yamauchi, C. Y. Hong, Y. H. Yang, Y. H. Liang, T. Funatsu, M. Tsunoda, *Chem. Commun.* **2011**, *47*, 5232–5234.
- [26] a) P. A. Connor, A. J. McQuillan, *Langmuir* **1999**, *15*, 2916–2921; b) H. Suzuki, T. Amano, T. Toyooka, Y. Ibuki, *Environ. Sci. Technol.* **2008**, *42*, 8076–8082.
- [27] K. N. Yu, S. M. Lee, J. Y. Han, H. Park, M. A. Woo, M. S. Noh, S. K. Hwang, J. T. Kwon, H. Jin, Y. K. Kim, P. J. Hergenrother, D. H. Jeong, Y. S. Lee, M. H. Cho, *Bioconjugate Chem.* **2007**, *18*, 1155–1162.
- [28] K. Kim, Y. M. Lee, H. B. Lee, K. S. Shin, *Biosens. Bioelectron.* **2009**, *24*, 3615–3621.
- [29] P. Liu, R. Liu, G. Guan, C. Jiang, S. Wang, Z. Zhang, *Analyst* **2011**, *136*, 4152–4158.
- [30] X. Gao, W. C. Chan, S. Nie, *J. Biomed. Opt.* **2002**, *7*, 532–537.
- [31] N. Leopold, B. Lendl, *J. Phys. Chem. B* **2003**, *107*, 5723–5727.
- [32] A. F. Demirörs, A. van Blaaderen, A. Imhof, *Langmuir* **2010**, *26*, 9297–9303.

Received: November 14, 2011
Published online: March 29, 2012